Deformation, orientation, and medium effects in ^{16,19}C + C reactions

M. Rashdan
Islamic University, Faculty of Science, Physics Department, Madinah, Saudi Arabia
(Received 9 July 2012; revised manuscript received 18 August 2012; published 9 October 2012)

The shape, deformation, and orientation dependence as well as in-medium effects are investigated for the reaction cross sections of ^{16,19}C + C systems within the optical Glauber theory, which is currently used to deduce information about the structure of exotic nuclei. A density- and energy-dependent effective nucleon-nucleon reaction cross section is used locally to study in-medium effects. The projectile deformation is treated by a deformed Fermi shape with quadrupole and hexadecapole deformations, where the deformation parameters of ^{16}C and ^{19}C are calculated from the Lagrangian density of the relativistic mean-field (RMF) model. A strong prolate deformation is predicted for ^{16}C while a more stronger oblate shape is predicted for ^{19}C. Medium effects are found to be important for extracting reliable information about the nuclear densities and radii. The deformations and orientations strongly affected the reaction cross section. The difference in the reaction cross section calculated at orientation angle $\pi/2$ and at zero degree is of the order of 400 mb. The integrated reaction cross section over all orientation angles (angle average), including in-medium effects, predicted the experimental reaction cross section of ^{19}C + ^{12}C. For ^{16}C + ^{12}C the rms radius of ^{16}C is increased to about 7% than that predicted by the RMF model in order to predict the experimental data. This greater increase in the rms radius of ^{16}C, to about 3 fm, indicates a neutron halo structure for this nucleus. The deduced spherical Fermi distributions which fit the experimental data of ^{16,19}C + ^{12}C systems are in fact a prediction of the angle average cross sections.

DOI: 10.1103/PhysRevC.86.044610 PACS number(s): 25.70.−z, 21.60.−n, 24.10.−i

I. INTRODUCTION

The reaction cross-section measurements at intermediate and high energies have been extensively used to estimate the size and matter distributions of unstable light exotic nuclei that are produced in high-energy fragmentation reactions [1–10]. The optical-limit approximation to Glauber theory [11–15] has been used in these analyses. However, in most of these calculations deformation as well as medium effects have been neglected. For example, the reaction cross section of a ^{19}C projectile at an incident energy of 960 MeV/nucleon on a ^{12}C target has been studied in Ref. [15] using the few-body Glauber theory as well as the optical limit and it has been found that the reaction cross section calculated in the few-body Glauber model is smaller than that calculated in the optical limit and the difference between the two calculated cross sections depends on the model assumed for the ground-state configuration of ^{19}C and the one-neutron separation energy, which is not well known.

The reaction cross section of a ^{16}C projectile on ^{12}C has been measured in Ref. [16] using a different experimental method and the Glauber model has been used to study this reaction. The larger enhancement of the ^{16}C reaction cross section at the low energy has been used to investigate the density distribution of ^{16}C, assuming a spherical configuration.

In this work we study the effect of deformation and orientation as well as medium effects on the reaction cross section of ^{16,19}C + ^{12}C at intermediate and high energies. This study is interested in answering the important question of whether intrinsic deformation of neutron-rich nuclei should be taken into account in determining their structure from measurements of reaction cross sections. Indeed, can we get information about the deformation parameters from these measurements? To answer these questions we used the optical limit in this calculation where deformations and orientation angles can directly be included through the nuclear densities. Medium effects are included through a density- and energy-dependent effective nucleon-nucleon reaction cross section. The projectile deformation is treated by a deformed Fermi shape with quadrupole and hexadecapole deformations, where the deformation parameters β_2 and β_4 of ^{16}C and ^{19}C are derived from the Lagrangian density of the relativistic mean-field (RMF) model using the relativistic effective interaction NL-RA1, which well describes spherical [17] and deformed nuclei [18]. Other interactions like NL3 and NLSH are also used for comparison.

In fact, the ^{19}C nucleus has attracted much attention after it was suggested to be a one-neutron halo candidate following the observed narrow momentum distribution Ref. [19]. The small one-neutron separation energy for ^{19}C, which suffers from a large uncertainty ($S_n = 162 \pm 112$ keV [20], $S_n = 240 \pm 100$ keV [21], or $S_n = 530 \pm 130$ keV [22]), could also provide important but incomplete evidence for the halo structures. The ground-state spin parity of this nucleus is not well determined experimentally. Some measurements suggested the presence of a halo structure ground-state configuration of ^{19}C [23] as well as of ^{16}C [16]. Experimental reinvestigation of the longitudinal momentum distribution of this nucleus with a ^{12}C target around 910 MeV/nucleon [24], however, presents a different view, where the narrowing of the shell gap has been found to change the ground-state spin from $1/2^+$ to $5/2^+$. On the other hand, self-consistent models of nuclear structure such as deformed relativistic mean-field and Hartree-Fock calculations would also provide important information about the structure of ^{16}C and ^{19}C. The paper is organized as follows: The RMF description and calculation of ^{16}C and ^{19}C isotopes are presented in Sec. II. The description of the Glauber-type calculation is presented in Sec. III. The results for reactions between carbon isotopes are presented in Sec. IV.

II. RELATIVISTIC MEAN-FIELD DESCRIPTION OF ^{16,19}C ISOTOPES

The Lagrangian density of the RMF theory is used to derive the deformation parameters and rms radii of the neutron-rich carbon nuclei, using a deformed configuration and employing the NL-RA1 interaction [17,18]. In this Lagrangian, Dirac nucleons interact with the scalar self-coupling σ-meson field Φ, the self-coupling neutral vector ω-meson field $\mathbf{V}^{\mu}(\mu = 0, 1, 2, 3)$, the isovector-vector ρ-meson field $\overrightarrow{\rho}^{\mu}$, and the electromagnetic fields A^{μ}:

$$\begin{aligned} L = {} & \overline{\psi_i}(\gamma^{\mu} i\partial_{\mu} - M)\psi_i + \frac{1}{2}\partial^{\mu}\Phi\partial_{\mu}\Phi - \frac{1}{2}m_{\sigma}^2\Phi^2 - \frac{1}{3}b_2\Phi^3 \\ & - \frac{1}{4}b_3\Phi^4 - g_s\overline{\psi_i}\psi_i\Phi \\ & - \frac{1}{4}\Omega^{\mu\nu}\Omega_{\mu\nu} + \frac{1}{2}m_{\omega}^2\mathbf{V}^{\mu}\mathbf{V}_{\mu} - g_{\omega}\overline{\psi_i}\gamma^{\mu}\psi_i\mathbf{V}_{\mu} \\ & - \frac{1}{4}\overrightarrow{\mathbf{B}}^{\mu\nu}\overrightarrow{\mathbf{B}}_{\mu\nu} + \frac{1}{2}m_{\rho}^2\overrightarrow{\rho}^{\mu}\overrightarrow{\rho}_{\mu} - g_{\rho}\overline{\psi_i}\gamma^{\mu}\overrightarrow{\tau}\psi_i\overrightarrow{\rho}_{\mu} \\ & - \frac{1}{4}\mathbf{F}^{\mu\nu}\mathbf{F}_{\mu\nu} - e\overline{\psi_i}\gamma^{\mu}\frac{1+\tau_{3i}}{2}\psi_i\mathbf{A}_{\mu}. \end{aligned} \tag{1}$$

Vectors in isospin space are denoted by arrows. The Dirac spinor ψ_i represents the nucleon with mass M and oscillates with the single-particle energies ϵ_i. m_{σ}, m_{ω}, and m_{ρ} are the masses of the σ-meson, the ω-meson, and the ρ-meson, respectively. The meson-nucleon coupling constants, g_{σ}, g_{ω}, and g_{ρ}, and the meson masses are parameters adjusted to fit nuclear matter data and some static properties of finite nuclei. τ_3 is the third component of the isospin. The field tensors of the vector mesons and the electromagnetic fields are defined as

$$\Omega^{\mu\nu} = \partial^{\mu}\mathbf{V}^{\nu} - \partial^{\nu}\mathbf{V}^{\mu}, \tag{2}$$

$$\vec{B}^{\mu\nu} = \partial^{\mu}\vec{\rho}^{\,\nu} - \partial^{\nu}\vec{\rho}^{\,\mu} - g_{\rho}(\vec{\rho}^{\,\mu}\times\vec{\rho}^{\,\nu}), \tag{3}$$

$$F^{\mu\nu} = \partial^{\mu}\mathbf{A}^{\nu} - \partial^{\nu}\mathbf{A}^{\mu}. \tag{4}$$

From the relativistic Lagrangian density (1), we get the mean-field equations for mesons and nucleons. These equations are solved by expanding the upper and lower components of the Dirac spinors and the boson field wave functions with some initial deformation in a reasonably large deformed harmonic-oscillator basis [18]. For light nuclei the number of shells for both fermionic and bosonic wave functions is taken to be 12. The difference in the results with 14 shells is negligible and therefore calculations for isotopes with $Z = 10$–24 were performed in a 12-shell harmonic-oscillator expansion. The set of coupled Dirac, Klein-Gordon, and Poisson field equations, which are obtained from the RMF Lagrangian density, Eq. (1), by means of the variational principle, are solved numerically by the self-consistent iteration method for the case of deformed axially symmetric systems of nucleons to obtain Dirac spinors ψ_i of the nucleons and the fields of σ, ρ, and ω mesons and the photon. The quadrupole deformation parameter β is evaluated from the resulting quadrupole moment Q using the formula

$$Q = Q_n + Q_p = \sqrt{\frac{9}{5\pi}}AR^2\beta, \tag{5}$$

where $R = 1.2A^{1/3}$ fm.

Pairing is a very crucial quantity for open-shell nuclei in determining the nuclear properties, although it does not contribute significantly to the lighter-mass region. The constant-gap, BCS-pairing approach is reasonably applicable. In order to take care of the pairing effects in this work, we use the constant gap for the proton and neutron, as given in Refs. [10,25]:

$$\Delta_p = CB_s e^{sI - tI^2}/Z^{1/3}, \tag{6}$$

$$\Delta_n = CB_s e^{-sI - tI^2}/A^{1/3}, \tag{7}$$

with $C = 5.72$, $s = 0.118$, $t = 8.12$, $B_s = 1$, and $I = (N - Z)/(N + Z)$. This type of prescription for pairing effects, both in the RMF- and Skyrme-based approaches, has already been used by many authors, and it is shown that the results for binding energies and quadrupole deformations are almost identical with the predictions of the relativistic Hartree-Bogoliubov (RHB) approach [10,25]. The results for the binding energies, radii, quadrupole, and hexadecapole deformation parameters calculated using NL-RA1 of ^{16}C and ^{19}C are listed in Table I. Tables II and III present the results of NL3 and NLSH interactions, which nearly give similar results. As seen in Table I we get an oblate shape for ^{19}C with $\beta_2 = -0.426$ and $\beta_4 = 0.185$ and prolate shape for ^{16}C with $\beta_2 = 0.33$ and $\beta_4 = 0.15$. The large negative value of β_2 refers to the strong oblate shape predicted for ^{19}C. The rms radii are of the order 3 fm for ^{19}C and 2.778 fm for ^{16}C. There is another but higher minima with prolate shape for ^{19}C with $\beta_2 = 0.377$ and $\beta_4 = 0.01$ and with a slightly smaller rms radius of 2.97 fm. For the case of ^{16}C we get at the second-highest minima an oblate shape with $\beta_2 = -0.19$ and $\beta_4 = 0.054$ nearly with the same rms radius of 2.775 fm.

TABLE I. The predictions of NL-RA1 relativistic interaction for the binding energy, radii, and deformation parameters for ^{16}C and ^{19}C. For each nucleus the first row gives the results at the first minima, while the second gives the results of the second minima.

Nucleus	E (MeV)	r_c (fm)	r_p (fm)	r_n (fm)	r_M (fm)	β_2	β_4
^{16}C	113.1	2.6	2.5	2.93	2.778	0.33	0.15
	112.44	2.58	2.49	2.93	2.775	−0.19	0.054
^{19}C	120.9	2.62	2.52	3.17	2.98	−0.426	0.186
	119.3	2.6	2.5	3.17	2.97	0.337	0.01

TABLE II. Same as Table I but for the NL3 interaction.

Nucleus	E (MeV)	r_c (fm)	r_p (fm)	r_n (fm)	r_M (fm)	β_2	β_4
^{16}C	112	2.61	2.51	2.95	2.8	0.33	0.17
	111.4	2.6	2.5	2.95	2.78	−0.188	0.066
^{19}C	119.7	2.62	2.53	3.19	3	−0.43	0.19
	118.2	2.6	2.5	3.18	2.98	0.38	0.008

III. DESCRIPTION OF GLAUBER-TYPE CALCULATION

The reaction cross sections of $^{16,19}\mathrm{C} + {}^{12}\mathrm{C}$ are calculated assuming a deformed Fermi shape for both ^{16}C and ^{19}C with quadrupole and hexadecapole deformations. We define the orientation angle β as the angle between the symmetry axis z' of the projectile nucleus and the line joining the centers of the two colliding nuclei; that is, the vector $\mathbf{R}$, where $R = \sqrt{b^2 + Z^2}$ and b is the impact parameter. The symmetry axis of the projectile z' is assumed to be parallel to the z coordinate, and R is assumed to be lying in the x-z plane.

The optical-limit reaction cross section for a fixed orientation angle β of the incident projectile can be written as

$$\sigma_R(\beta) = 2\pi \int_0^\infty db\, b[1 - e^{-\chi(b,\beta)}], \tag{8}$$

where

$$\chi(b,\beta) = \int dZ \int d^3r \overline{\sigma}_{\mathrm{NN}}(E,\rho)\rho_P(|\,\mathbf{r} - \mathbf{R}\,|)\rho_T(\mathbf{r}), \tag{9}$$

where $\overline{\sigma}_{\mathrm{NN}}(E, \rho = \rho_T(\mathbf{r}) + \rho_P(|\,\mathbf{r} - \mathbf{R}\,|))$ is the isospin average nucleon-nucleon (NN) cross section, which depends on the total density of the two interacting nuclei and incident energy. The functional form of this dependence can be written as [26]

$$\begin{aligned}
\overline{\sigma}_{\mathrm{NN}}(E,\rho) &= \frac{Z_P N_T \sigma_{nn} + Z_P Z_T \sigma_{pp} + N_P Z_T + N_T Z_P \sigma_{np}}{A_P A_T}, \\
\sigma_{pp} &= \sigma_{nn} = f_1(u)\,\frac{1 + 7.772E^{0.06}\rho^{1.48}}{1 + 18.01\rho^{1.46}}, \\
\sigma_{np} &= f_2(u)\,\frac{1 + 20.88E^{0.04}\rho^{2.02}}{1 + 35.86\rho^{1.9}}, \\
f_1(u) &= 13.73 - 15.04u^{-1} + 8.76u^{-2} + 68.67u^4, \\
f_2(u) &= -70.67 - 18.18u^{-1} + 25.26u^{-2} + 113.85u,
\end{aligned} \tag{10}$$

where E is the energy per nucleon of the projectile and the velocity $u = (1 - 1/\gamma^2)^{1/2}$, where $\gamma = E/931.5 + 1$. In Ref. [26], a global constant central density $\rho(0)$ is considered for the density dependence of the average NN cross section. This global density approximation has been tested in Ref. [27] and has been found to be inadequate. In this work we used the exact local density dependence of the NN cross section in the expressions (10), where the density is taken as the sum of the target and projectile density in each volume element being considered (i.e., the local density at each point along the trajectory).

It is worth mentioning that the present approximation of the choice of the coordinate axes, where the symmetry axis makes an angle β with the line joining the two centers of the two nuclei and this axis is parallel to the z axis, is called the rotating-frame approximation and is normally used in calculations of low-energy fusion reactions [28] and not in high-energy reactions. It is used in this work for convenience and is tested by comparing with the work of Christley and Tostevin [29]. In that work the frozen-geometry approximation is used, where the symmetry axis makes two orientation angles (Θ, Φ) with the coordinates (see Fig. 1 in Ref. [29] for details). This method is more appropriate for high-energy reactions. However, the application of the frozen-geometry approximation would be very time consuming because of the density dependence of the effective NN cross section. In the present work the multidimensional integrals of the reaction cross sections, including integration over orientations (angle average), are carried out numerically without multipole expansion in a wider range of energy from 20 to 2000 MeV/u. Both proton and neutron densities of the projectile are considered, with quadrupole and hexadecapole deformations. The local density-dependent isospin average NN cross section $\sigma_{\mathrm{NN}}(E, \rho)$ is considered exactly. The multipole expansion for the nuclear densities used in Ref. [29] cannot be applied in the present work due to the nontrivial dependence of $\sigma_{\mathrm{NN}}(E, \rho)$ on the total density.

To test and compare the present method with that of Ref. [29], we calculated the reaction cross section of $^{17}\mathrm{Ne} + {}^{12}\mathrm{C}$ at 700 MeV and considered the same fixed value for the isospin average NN cross section taken there: $\sigma_{\mathrm{NN}} = 4.087$ fm^2. As in Ref. [29], for ^{12}C a Gaussian density is used with a rms radius of 2.32 fm and for ^{17}Ne a two-parameter Fermi shape is used with a fixed diffuseness, $a = 0.564$ fm, and with a quadrupole deformation β_2. For the spherical case $\beta_2 = 0$ and the half density, the radius is taken to be

TABLE III. Same as Table I but for the NLSH interaction.

Nucleus	E(MeV)	r_c (fm)	r_p (fm)	r_n (fm)	r_M (fm)	β_2	β_4
^{16}C	111.34	2.287	2.49	2.91	2.76	0.332	0.18
	110.8	2.58	2.48	2.91	2.75	−0.211	0.074
^{19}C	118.6	2.6	2.5	3.15	2.96	−0.42	0.18
	117	2.58	2.48	3.14	2.95	0.37	0.0017

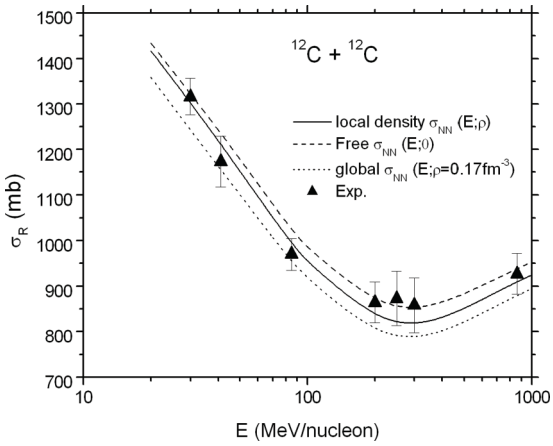

FIG. 1. Reaction cross section for the $^{12}C + ^{12}C$ system plotted against incident energy calculated using local (solid) and global (dotted) density-dependent nucleon-nucleon cross section. The dashed line represents the reaction cross section calculated using the free nucleon-nucleon cross section.

$R_0 = 2.17$ fm to get the rms radius of 2.682 fm. The reaction cross section calculated in the present approach is found to be 1065.3 mb, which is the same value obtained in Ref. [29] (1065.7 mb).

For the deformed case, the diffuseness is fixed to $a = 0.564$ fm and $\beta_2 = 0.2289$, as in Ref. [29]. With $R_0 = 2.14$ fm the rms radius is 2.68 fm, as for the spherical case. In this case, the angle average reaction cross section is found to be 1058.8 fm, which is also very close to that obtained in Ref. [29] (1057.6 mb).

Finally, the case of orientation angle $\beta = \pi/2$ can be obtained from the general case by putting $\Theta = \Phi = \pi/2$ in Eq. (13) of Ref. [29]. For this case they obtained a cross section of 1006.3 mb. The calculated cross section in this work for the same case (i.e., $\beta = \pi/2$) is found to be 1009 mb. The small difference could be due to the difference in R_0 which is increased here to 2.14 fm to get the rms of Ref. [29]

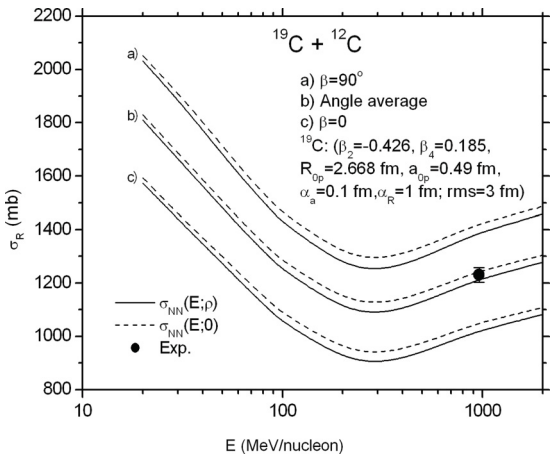

FIG. 2. Reaction cross section of $^{19}C + ^{12}C$ system as a function of incident energy per nucleon at orientation angles $\beta = 0$ and $\beta = 90$ calculated with (solid lines) and without (dashed lines) including in-medium effects.

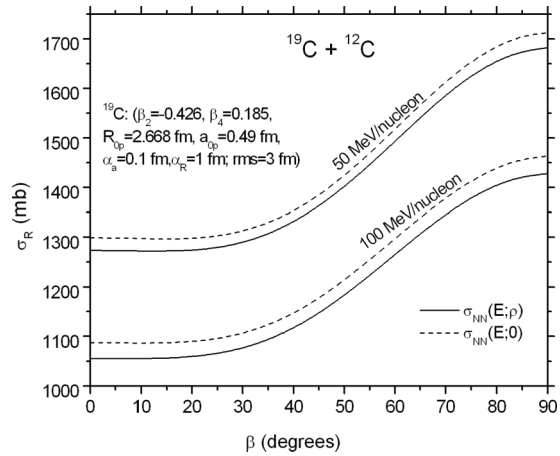

FIG. 3. Reaction cross section of $^{19}C + ^{12}C$ system as a function of orientation angle β calculated at incident energy 50 MeV/nucleon and 100 MeV/nucleon with and without including medium effects.

(2.68 fm). If we use the same value of Ref. [29] ($R_0 \cong 2.11$ fm), we get the same value of the cross section, 1006.3 mb. The central density is determined by the normalization condition: $\rho_0 = 0.251\,087$ fm^{-3}.

These results show that the present approximation for the choice of the coordinate axes in the Glauber model calculations can be considered as a reasonable approximation. However, we hope to consider the general case used in Ref. [29] for the description of the coordinate axes in future work.

IV. RESULTS FOR REACTIONS BETWEEN CARBON ISOTOPES

The nuclear density of the target ^{12}C is taken to be a two-parameter Fermi shape:

$$\rho^T_{i=p,n}(\mathbf{r}) = \frac{\rho^T_{0i}}{1 + e^{(r-R^T_{0i})/a^T_{0i}}}. \tag{11}$$

The neutron and proton diffuseness parameters for ^{12}C are taken to be equal, as well as the half-density radii, and these parameters are adjusted to reproduce the rms radius

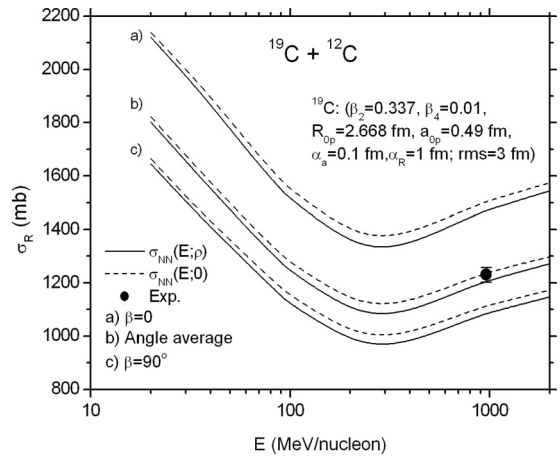

FIG. 4. Same as Fig. 2, but for $\beta_2 = 0.337$ and $\beta_4 = 0.01$.

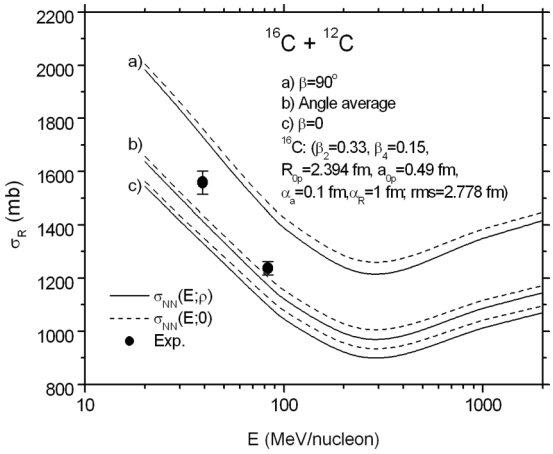

FIG. 5. Same as Fig. 2, but for ^{16}C + ^{12}C system.

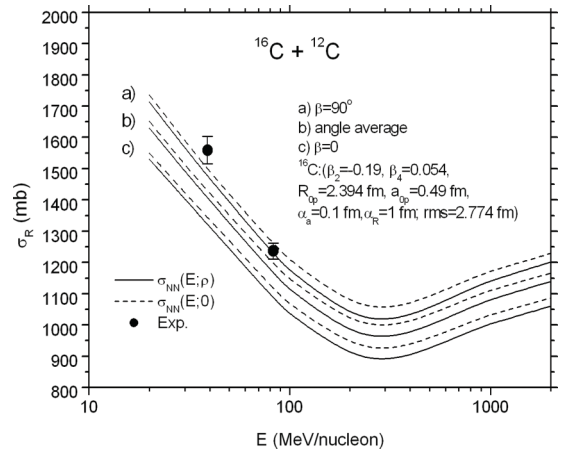

FIG. 7. Same as Fig. 4, but for ^{16}C + ^{12}C system.

of 2.45 fm of ^{12}C as well as the experimental ^{12}C + ^{12}C reaction cross section between 100 and 1000 MeV/nucleon, calculated including medium effects $[\sigma_{\rm NN}(E,\rho)]$ with local density-dependent isospin average NN cross section, as shown in Fig. 1 by the solid line. The dashed and dotted lines are the reaction cross section of ^{12}C + ^{12}C calculated using free $[\sigma_{\rm NN}(E,\rho=0)]$ and global $[\sigma_{\rm NN}(E,\rho=\rho_0=0.17\ {\rm fm}^{-3})]$. The half-density radius of ^{12}C is taken to be 2.2 fm and the diffuseness 0.475 fm, which better fits the σ_R of ^{12}C + ^{12}C and the rms radius of ^{12}C and the reaction cross section. As shown from Fig. 1, the interaction used a medium global density $\sigma_{\rm NN}(E,\rho_0=0.17\ {\rm fm}^{-3})$, which largely reduced the reaction cross section in disagreement with the data. A similar result has been obtained by Warner *et al.* Ref. [27] using Gaussian densities and a different density-dependent $\sigma_{\rm NN}$. One also notices that medium effects on the NN cross section slightly reduces the reaction cross section at all energies where the data are better described at lower energies when using a density-dependent NN cross section while at high energy both the free and medium NN cross section can describe the data.

For ^{16}C + ^{12}C and ^{19}C + ^{12}C reactions, a deformed Fermi shape with quadrupole and hexadecapole deformation parameters is assumed for the projectile; namely,

$$\rho^P_{i=p,n}(\mathbf{r}') = \frac{\rho^P_{0i}}{1+e^{\left[r'-R^P_i(\theta')\right]/a^P_{0i}}}, \tag{12}$$

where

$$R^P_i(\theta') = R^P_{0i}[1+\beta_2 Y_{20}(\theta')+\beta_4 Y_{40}(\theta')], \tag{13}$$

$$\mathbf{r}' = \mathbf{r}-\mathbf{R}, \quad \mathbf{r}'^2 = \mathbf{r}^2+\mathbf{R}^2-2rR\cos\alpha, \tag{14}$$

$$\cos\theta' = (r\cos\theta - R\cos\beta)/r',$$
$$\cos\alpha = \cos\theta\cos\beta+\sin\theta\sin\beta\cos\phi, \tag{15}$$

In the deformed Fermi density Eqs. (12)–(15), we used the deformation parameters, appearing in Eq. (13), β_2 and β_4 as calculated from the RMF theory, employing NL-RA1 interaction. These deformation parameters are listed in Table I. The other parameters of the deformed Fermi shape, like diffuseness and radii, are adjusted to reproduce the rms radius as predicted in Table I by the RMF calculations. In this case, the proton radius parameter R^P_{0p} appearing in the deformed Fermi shape is assumed to take the value 2.394 fm for ^{16}C and 2.668 fm for ^{19}C. The neutron radius parameter R^P_{0n} is

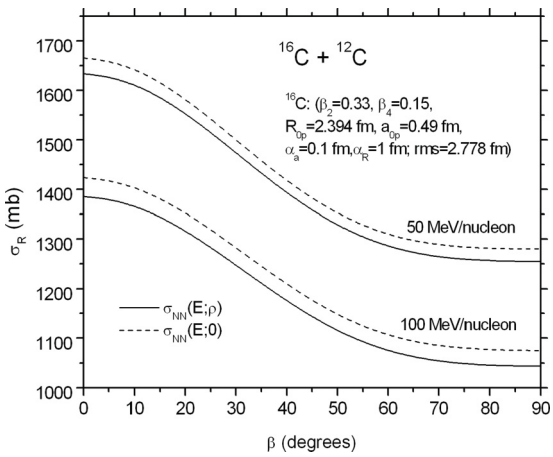

FIG. 6. Same as Fig. 3, but for ^{16}C + ^{12}C system.

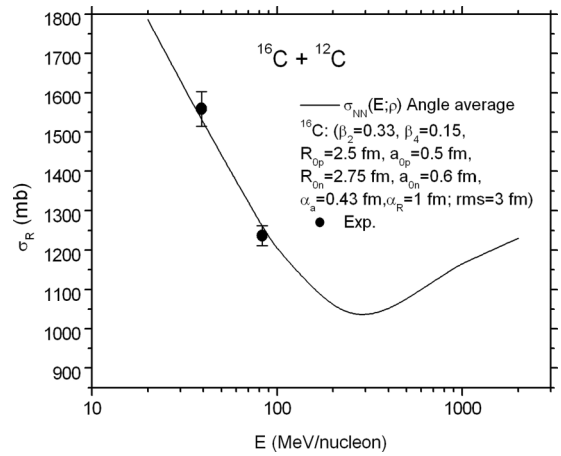

FIG. 8. Angle-average cross section which fit experimental data (see text for details).

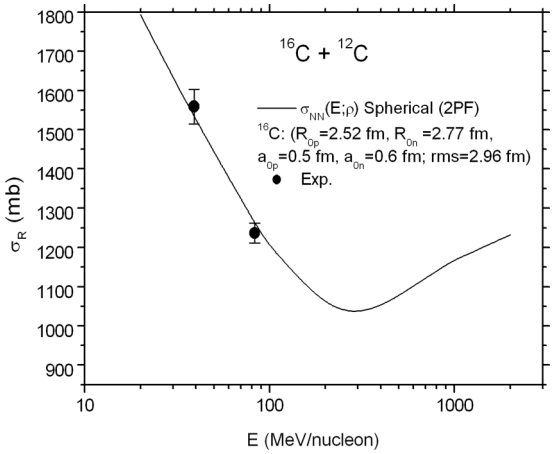

FIG. 9. Same as Fig. 8, but data are fit by a spherical 2PF density distribution.

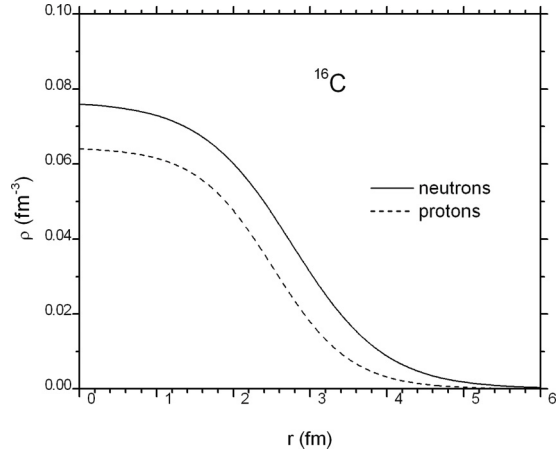

FIG. 10. Spherical 2PF density distribution of ^{16}C which fit experimental cross section plotted against the distance r from the center.

assumed to increase more than the proton parameter by the neutron excess [30]; namely,

$$R_{0n}^{P} = R_{0p}^{P} + \alpha_R I. \tag{16}$$

The proton diffuseness parameter a_{0p}^{P} for both ^{16}C and ^{19}C is taken to 0.49 fm and the neutron diffuseness is assumed to increase more than the proton diffuseness also by the neutron excess; namely,

$$a_{0n}^{P} = a_{0p}^{P} + \alpha_a I, \tag{17}$$

where α_R is a scale parameter taken to be 1 fm [30] and the scale factor α_a is taken to be 0.1 fm, in order to account for the longer tail of the neutron-density distribution. With these parameters of the deformed Fermi shape of the nuclear densities we get for the rms radius

$$\langle r^2 \rangle^{1/2} = \frac{\int r^2 \rho\,(r,\theta)\, d\Omega}{\int \rho\,(r,\theta)\, d\Omega}, \tag{18}$$

the value 3 fm for the oblate shape of ^{19}C and 2.778 fm for the prolate shape of ^{16}C. These results for the rms radii are consistent with the RMF calculations of rms matter radii, as seen from Table I.

The assumed relations Eqs. (16) and (17) are in fact a simple estimation for the neutron diffuseness and half-density radius of a neutron-rich nucleus, which could be interpreted as a first-order expansion of the neutron diffuseness and half-density radius in terms of the proton ones and the neutron excess. The total density is taken as the sum of target and projectile density distributions at each separation distance and each of target and projectile density is taken as the sum of proton and neutron densities.

Figure 2 shows the reaction cross section of the ^{19}C + ^{12}C system as a function of the incident energy per nucleon calculated at orientation angles $\beta = 0$ and $\beta = 90$ with (solid lines) and without (dashed lines) including in-medium effects; that is, with a local density-dependent NN cross section $\sigma_{\rm NN}(E; \rho = \rho_T(\mathbf{r}) + \rho_P(\mathbf{r}'))$ and with a free NN cross section $\sigma_{\rm NN}(E; \rho = 0)$. Figure 3 shows the reaction cross section of ^{19}C + ^{12}C system as a function of the orientation angle β calculated at incident energies of 50 MeV/nucleon and 100 MeV/nucleon with and without including in-medium effects. As shown from these figures the reaction cross section strongly depends on deformation and orientation, where the difference between the cross section calculated at zero orientation angle and at $\pi/2$ is of the order of 400 mb. This is due to the strong deformation of ^{19}C. The lowest reaction cross section exists at an orientation angle $\beta = 0$ and the largest at $\beta = \pi/2$ due to the strong oblate deformation of ^{19}C. This behavior is inverted if β_2 is positive (prolate shape), as shown from Fig. 4, where the deformation parameters at the second minima, listed in Table I, are used in the calculation of the reaction cross section.

The integrated reaction cross section (angle average) over all orientation angles,

$$\sigma_R = \frac{1}{4\pi} \int \sigma_R\,(\beta)\, 2\pi \sin\beta d\beta, \tag{19}$$

is shown in Figs. 2 and 4 by the curves denoted by (b). These angle-average curves with in-medium effects fit well the experimental data of ^{19}C + ^{12}C. Figures 5, 6, and 7 are the same as Figs. 2, 3, and 4, respectively, but for the ^{16}C + ^{12}C system. As shown from these figures, an inverse behavior of the reaction cross section to that of the case of ^{19}C + ^{12}C with

TABLE IV. Parameters of the spherical (2PF) density distributions of ^{16}C and ^{19}C which fit the reaction cross sections.

Nucleus	R_{0p} (fm)	R_{0n} (fm)	a_{0p} (fm)	a_{0n} (fm)	α_R (fm)	α_a (fm)	rms (fm)
^{16}C	2.52	2.77	0.5	0.608	1	0.43	2.96
^{19}C	2.7	3	0.5	0.537	1	0.1	3

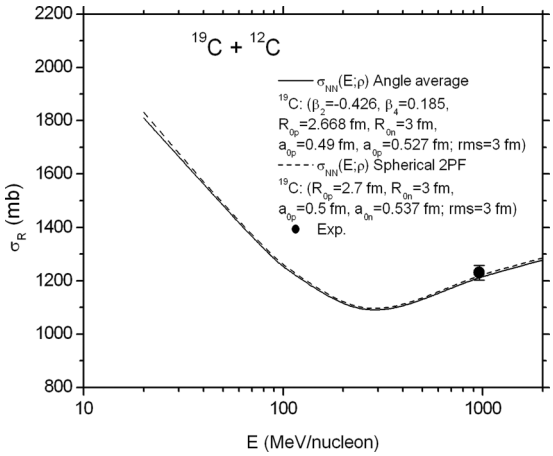

FIG. 11. Same as Fig. 9, but for $^{19}C + ^{12}C$ system.

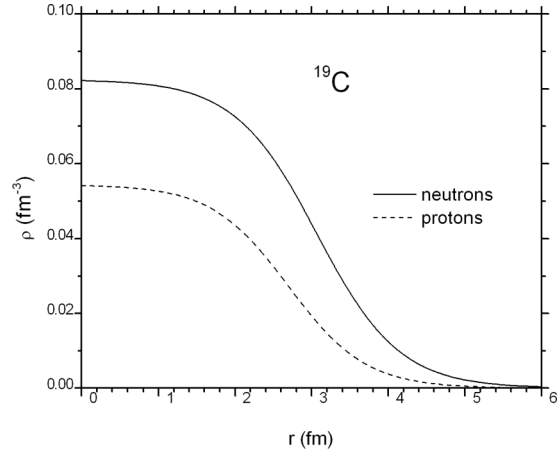

FIG. 12. Same as Fig. 10, but for ^{19}C nucleus.

respect to orientation angles is obtained since the quadrupole deformation parameter of ^{16}C is inverted. One also notices from Fig. 7 that the difference in the cross sections at $\beta = 0$ and $\beta = \pi/2$ is strongly reduced compared to that of Fig. 5 since the absolute value of the deformation parameters are strongly reduced at the second minima. On the other hand, in both cases the angle-average cross section does not fit the experimental cross section, as shown from Figs. 5 and 7, where the experimental cross section is much higher at lower energies. This could be due to the fact that the ^{16}C nucleus has a halo structure and thus the rms radius should be larger than that predicted by RMF calculations of this nucleus. Thus we modify the parameters of the density distribution to increase the rms radius in order to fit the experimental data by increasing both the radii and diffuseness of the deformed density distribution. In this case R_{0p} is increased from about 2.4 to 2.5 fm with the same scale factor $\alpha_R = 1$ fm. Thus the neutron radius parameter R_{0n} is increased from 2.644 to 2.75 fm. The proton diffuseness a_{0p} is slightly increased from 0.49 to 0.5 fm while the neutron diffuseness is more increased from 0.515 to 0.61 fm (α_a is increased from 0.1 to 0.43 fm). With these modifications of the parameters of the density distribution of ^{16}C the rms radius is increased from 2.778 to 3 fm and the experimental reaction cross section is well fit by the angle-average cross section (including medium effects), as shown in Fig. 8. This increasing in the rms as deduced from the experimental data indicate the neutron skin or halo structure of ^{16}C.

It is also important to fit the experimental cross section by a spherical two-parameter Fermi (2PF) shape. In this case we fix the diffuseness parameters to nearly that deduced from the deformed configuration of ^{16}C and increased R_{0n} and a_{0n} by the factors $\alpha_R = 1$ fm and $\alpha_a = 0.43$ fm, respectively, as for the deformed case. These parameters of the spherical shape are listed in Table IV for ^{16}C and ^{19}C. The rms radius of ^{16}C calculated by this spherical shape slightly decreased to 2.96 fm. The experimental cross section, as well as the angle-average cross section, are well fit by this spherical 2PF density, as shown in Fig. 9. The spherical 2PF density distribution which fit the experimental cross section is plotted in Fig. 10. This figure indicates a neutron halo structure of ^{16}C.

Figures 11 and 12 are the same as Figs. 9 and 10 but for $^{19}C + ^{12}C$. The proton radius of ^{19}C slightly increased from 2.667 to 2.7 fm and the proton diffuseness from 0.49 to 0.5 fm. The neutron radius and diffuseness are increased by a similar ratio as for the deformed case, where $\alpha_R = 1$ fm and $\alpha_a = 0.1$ fm. As shown from Fig. 11 the spherical 2PF shape fit both the angle-average cross section and experimental data of $^{19}C + ^{12}C$ very well as for the case of $^{16}C + ^{12}C$ but without increasing more in the neutron diffuseness, as for the case of ^{16}C. This could refer to a large neutron skin or a halo structure of ^{19}C. This large neutron skin of ^{19}C is shown in Fig. 12 for the predicted spherical Fermi distribution.

Finally, one can conclude that nuclear deformation and in-medium effects play an interesting rule in extracting information about the structure of exotic nuclei from nuclear reactions. The deformation parameters cannot be deduced from the present experimental data of reaction cross sections. The experimental data can only be fit by an angle-average cross section over all orientation angles or assuming a spherical configuration of both target and projectile. Information about the rms radius can be extracted from the data, which could indicate a neutron skin or a halo structure of exotic nuclei. In order to extract reliable information about nuclear shapes of exotic nuclei from experimental reaction cross sections it is important for future experiments to consider polarized exotic beams.

[1] I. Tanihata *et al.*, Phys. Rev. Lett. **55**, 2676 (1985); Phys. Lett. B **160**, 380 (1985); **206**, 592 (1988).

[2] T. Kubo, M. Ishihara, N. Inabe, H. Kumagai, I. Tanihata, and K. Yoshida, Nucl. Instrum. Methods Phys. Res., Sect. B **70**, 309 (1992).

[3] R. Kanungo, M. Chiba, N. Iwasa, S. Nishimura, A. Ozawa, C. Samanta, T. Suda, T. Suzuki, T. Yamaguchi, T. Zheng, and I. Tanihata, Phys. Rev. Lett. **88**, 142502 (2002).

[4] T. Suda *et al.*, RIKEN Accel. Prog. Rep. **35**, 42 (2002).

[5] K. Minomo, T. Sumi, M. Kimura, K. Ogata, Y. R. Shimizu, and M. Yahiro, Phys. Rev. C **84**, 034602 (2011); Phys. Rev. Lett. **108**, 052503 (2012).
[6] K. Tanaka *et al*., Phys. Rev. Lett. **104**, 062701 (2010).
[7] Mahesh K. Sharma, M. S. Mehta, and S. K. Patra, in *Proceedings of the DAE Symposium on Nuclear Physics*, edited by A. Chatterjee, D. C. Biswas, and P. Shukla, Vol. 56 (University of Andhra, Visakhapatnam, 2011), p. 578.
[8] Y. Urata, K. Hagino, and H. Sagawa, Phys. Rev. C **83**, 041303(R) (2011).
[9] M. Takechi *et al*., Phys. Lett. B **707**, 357 (2012).
[10] A. Shukla, Sven A. Berg, and S. K. Patra, J. Phys. G **38**, 095103 (2011).
[11] R. J. Glauber, in *High-Energy Collision Theory, Lectures in Theoretical Physics*, edited by W. E. Brittin and L. G. Dunham (Interscience, New York, 1985).
[12] Y. Ogawa, K. Yabana, and Y. Suzuki, Nucl. Phys. A **543**, 722 (1992); J. S. Al-Khalili and J. A. Tostevin, Phys. Rev. Lett. **76**, 3903 (1996).
[13] J. S. Al-Khalili, J. A. Tostevin, and I. J. Thompson, Phys. Rev. C **54**, 1843 (1996).
[14] J. A. Tostevin and J. S. Al-Khalili, Nucl. Phys. A **616**, 418c (1997).
[15] J. A. Tostevin and J. S. Al-Khalili, Phys. Rev. C **59**, R5 (1999).
[16] T. Zheng *et al*., Nucl. Phys. A **702**, 103 (2002).
[17] M. Rashdan, Phys. Rev. C **63**, 044303 (2001).
[18] M. Rashdan, Int. J. Mod. Phys. E **21**, 2106 (2012).
[19] D. Bazin *et al*., Phys. Rev. Lett. **74**, 3569 (1995); Phys. Rev. C **57**, 2156 (1998).
[20] G. Audi *et al*., Nucl. Phys. A **595**, 409 (1995).
[21] F. M. Marques *et al*., Phys. Lett. B **381**, 407 (1996).
[22] T. Nakamura *et al*., Phys. Rev. Lett. **83**, 1112 (1999).
[23] A. Ozawa *et al*., RIKEN Report No. RIKEN-AF-NP-294 (1998).
[24] T. Baumann *et al*., Phys. Lett. B **439**, 256 (1998).
[25] M. Del Estal, M. Centelles, X. Vinas, and S. K. Patra, Phys. Rev. C **63**, 024314 (2001).
[26] Cai Xiangzhow, Feng Jun, Shen Wenqing, Ma Yugang, Wang Jiansong, and Ye Wei, Phys. Rev. C **58**, 572 (1998).
[27] R. E. Warner, I. J. Thompson, and J. A. Tostevin, Phys. Rev. C **65**, 044617 (2002).
[28] M. Ismail and Kh. A. Ramadan, J. Phys. G **26**, 1621 (2000); J. Gomez-Camacho and R. C. Johnson, *ibid.* **12**, L235 (1986); O. Tanimura, Phys. Rev. C **35**, 1600 (1987).
[29] J. A. Christley and J. A. Tostevin, Phys. Rev. C **59**, 2309 (1999).
[30] M. Rashdan, Eur. J. Phys. A **16**, 371 (2003).